Simulation of ultrasound two-dimensional array transducers using a frequency domain model

Min Rao,[a] Tomy Varghese, and James A. Zagzebski
Department of Medical Physics, The University of Wisconsin—Madison, 1300 University Avenue, 1530 MSC, Madison, Wisconsin 53706

(Received 6 December 2007; revised 18 April 2008; accepted for publication 13 May 2008; published 18 June 2008)

Ultrasound imaging with two-dimensional (2D) arrays has garnered broad interest from scanner manufacturers and researchers for real time three-dimensional (3D) applications. Previously the authors described a frequency domain B-mode imaging model applicable for linear and phased array transducers. In this paper, the authors extend this model to incorporate 2D array transducers. Further approximations can be made based on the fact that the dimensions of the 2D array element are small. The model is compared with the widely used ultrasound simulation program FIELD II, which utilizes an approximate form of the time domain impulse response function. In a typical application, errors in simulated RF waveforms are less than 4% regardless of the steering angle for distances greater than 2 cm, yet computation times are on the order of 1/35 of those incurred using FIELD II. The 2D model takes into account the effects of frequency-dependent attenuation, backscattering, and dispersion. Modern beam-forming techniques such as apodization, dynamic aperture, dynamic receive focusing, and 3D beam steering can also be simulated. © *2008 American Association of Physicists in Medicine*. [DOI: 10.1118/1.2940158]

Key words: ultrasound, simulation, 2D array transducer, beam pattern, b-mode image

I. INTRODUCTION

Recently, two-dimensional (2D) array transducers have been studied extensively for applications in real time three-dimensional (3D) ultrasound imaging. A problem facing the development of 2D arrays is the complexity arising from the large number of array elements required in such transducers and the channel count needed for the ultrasound system. Thus, there have been a number of reports describing design, fabrication methods, and characterization of 2D transducer arrays.[1–4] To optimize image quality, many different array layouts and imaging techniques have been studied and applied.[5–8] Due to the complexity of implementing such systems, however, accurate and efficient simulation models are needed to evaluate beam properties and to determine optimum parameters for these devices. Models for computing transducer field patterns are thus essential in 2D array design.

Transducer field simulation methods can be divided into two categories: time domain and frequency domain models. Time domain simulations are based on utilizing the impulse response of a radiator at the chosen field points.[9,10] Closed form expressions for the impulse response function have been derived for many different geometries.[11,12] Since these functions are exact solutions, they should yield accurate results for the acoustic field. However, the impulse response generally exhibits discontinuities, which leads to the need for high temporal sampling rates to obtain accurate results for the field. Jensen and Svendsen[13] have simplified this method to reduce the computational complexity and have implemented their approach in the FIELD II program, a popular, linear propagation beam calculation program. Turnbull and Foster[14] have also performed an extensive study of beam patterns from 2D arrays using the time domain method.

Frequency domain simulation techniques are based on diffraction theory[15] for continuous waves. Various approximations can be made to reduce the computational complexity, and these lead to different degrees of accuracy and efficiency. Crombie *et al.*[16] studied the accuracy and efficiency of several beam simulation schemes. They concluded that in the frequency domain, the Fresnel approximation[15] yields the most accurate results for an unsteered array; however, the accuracy degrades with increasing steering angle. Li and Zagzebski[17] have developed a frequency domain B-mode imaging model for linear array transducers that is based on a less restrictive approximation than the Fresnel approximation. They also showed that this model yields accurate simulation results throughout the near field and far field, even when the beam is steered at large angles.

In this paper, we describe extensions of the 1D model developed by Li and Zagzebski[17] to study beam patterns and properties of B-mode images for 2D transducer arrays. We briefly describe the frequency domain model used for the simulation of beam patterns from 2D arrays. The accuracy of the model is demonstrated by comparison with results from FIELD II simulations. This model takes into account the effects of frequency-dependent attenuation, backscattering, and dispersion. Imaging techniques such as apodization, dynamic aperture, dynamic receive focusing, and 3D beam steering can also be simulated.

II. THEORY

II.A. Acoustic field of a single square element

For 2D ultrasound arrays, we assume that both the transducer element height and width are limited by the half-

wavelength constraint in order to avoid grating lobes in the 3D radiation field. In a homogeneous medium, if the transducer surface is embedded in an infinite rigid baffle, and is vibrating at an angular frequency ω [i.e., the velocity of the surface is $v(t)=u(\omega)e^{-i\omega t}$], the pressure field from a square element can be written as[18]

$$p_i(\vec{r},\omega) = -\frac{i\rho kcu(\omega)}{4\pi}A_0(\vec{r},\omega), \tag{1}$$

where

$$A_0(\vec{r},\omega) = \int_{-a/2}^{+a/2}\int_{-a/2}^{+a/2}\frac{e^{ik|\vec{r}-\vec{r}'|}}{|\vec{r}-\vec{r}'|}dx'\,dy'. \tag{2}$$

Here ρ is the density of the medium, c is the speed of sound, $k=\omega/c$ is the wave number, $\vec{r}$ is the field point, x', y', or $\vec{r}'$ denotes the coordinates of the source point on the surface of the transducer, and a is the dimension of the square element. The coordinate system for 2D array calculations is shown in Fig. 1. The task in any model for the beam from a transducer is to compute the 2D Rayleigh integral, such as described in Eq. (2), as efficiently as possible.

Define r to be the distance from the field point to the center of the element. Under the assumption that $r \gg a$, $|\vec{r}-\vec{r}'|$ can be expanded by

$$\begin{aligned}|\vec{r}-\vec{r}'| &= \sqrt{(x-x')^2+(y-y')^2+z^2}\\ &\approx r+\frac{1}{2r}(x'^2+y'^2-2yy'-2xx'),\end{aligned} \tag{3}$$

where x, y, and z are the coordinates of the field point. We can take advantage of the fact that if $a \approx \lambda/2$, terms on the order of $x'^2/2r$ are negligible for the integration in Eq. (2). This will introduce a phase error of $k(x'^2+y'^2)/2r < ka^2/4r \approx \pi\lambda/8r$ at most, which is smaller than 0.01 rad in the case when r is greater than 1 cm and the wavelength is around 250 μm (1500 $\mathrm{ms}^{-1}/6$ MHz).

Therefore,

$$|\vec{r}-\vec{r}'| \approx r-\frac{1}{r}(yy'+xx'). \tag{4}$$

Thus, Eq. (2) can be rewritten as

$$A_0(\vec{r},\omega) \approx \frac{a}{r}e^{ikr}\mathrm{sinc}\left(\frac{kxa}{2\pi r}\right)\mathrm{sinc}\left(\frac{kya}{2\pi r}\right). \tag{5}$$

The 2D Rayleigh integral now can be calculated using sinc functions. The computation time is greatly reduced using this approximation. Note that the y' integration must be done numerically when simulating 1D transducer arrays because the height of rectangular elements used in these devices usually is on the order of 1 cm (much larger than λ) and the term $y'^2/2r$ cannot be ignored.

II.B. Acoustic field from linear 2D transducer array elements

The field from 2D square array elements, which consist of $N \times N$ active elements, can be calculated using the following equations:

$$A(\vec{r},\omega) = \sum_{m=1}^{N}\sum_{n=1}^{N} a(m,n)A_{0m,n}(\vec{r},\omega)e^{-i\omega t(m,n,F_x,F_y,F_z)}, \tag{6}$$

where $a(m,n)$ is an apodization factor for the nth element in the mth row. The apodization factor can be as simple as Gaussian shaped, with maximum weighting of signals picked up from the center of the active aperture and the weighted falling off for elements at increasing distances from the center of the aperture. The parameter $t(m,n,F_x,F_y,F_z)$ is the time delay needed to steer and focus the beam at a spot (F_x,F_y,F_z). This can be written as

$$t(m,n,F_x,F_y,F_z) = \frac{1}{c}\left(\sqrt{\left[\left(n-\frac{N+1}{2}\right)d-F_x\right]^2+\left[\left(m-\frac{N+1}{2}\right)d-F_y\right]^2+F_z^2}-\sqrt{F_x^2+F_y^2+F_z^2}\right), \tag{7}$$

where d is the center-to-center distance between elements.

II.C. Generation of the RF signal

For pulse-echo imaging, under the assumption of local plane waves and the Born approximation, the total backscattered force from multiple scatterers detected by the transducer can be calculated using the following equation:[17]

$$F(\omega) = -\frac{i\rho}{4\pi}kcu(\omega)\sum_{j=1}^{M}\Phi(\omega)A^T(\vec{r}_j,\omega)A^R(\vec{r}_j,\omega), \tag{8}$$

where M is the total number of scatterers, $\Phi(\omega)$ quantifies the scattered amplitude, $A^T(\vec{r},\omega)$ models the transmitted

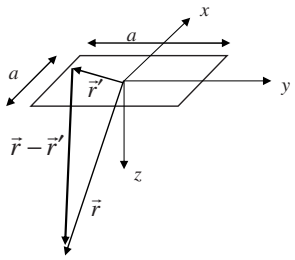

FIG. 1. Coordinate system used for computing the acoustic field from a square element. $\vec{r}$ is the field point, $\vec{r}'$ denotes the coordinates of the source point on the surface of the transducer, and a is the dimension of the square element.

beam profile, and $A^R(\vec{r},\omega)$ models the receiving profile. Dynamic receive focusing can be achieved by varying the F_x, F_y, F_z in the $A^R(\vec{r},\omega)$ term according the depth of the scatterer. The detailed derivation of Eq. (8) is presented by Li *et al.*[17] Here we assume the sizes of the scatterers are much smaller than the incident wavelength and the scatter number density is high enough to ensure Rayleigh statistics in the scattered echo signal waveform.[19] In our simulation, $\Phi(\omega)$ is calculated by assuming that the density of the scatterers is approximately equal to that of the surrounding medium, which can be written as

$$\Phi(\omega) = k^2 a_s^3 \frac{\kappa_e - \kappa}{3\kappa}, \tag{9}$$

where a_s is the radius of the scatterer, κ_e is the compressibility of the material of the scatterer, and κ is the compressibility of the medium.

In our simulation, $F(\omega)$ in Eq. (8) is calculated first by assuming that the initial amplitude of each frequency transmitted by the transducer is the same. In fact, the transducer transmits a short duration pulse with a limited bandwidth. Since we assume that the imaging process is linear, we simply calculate the frequency spectrum of the incident pulse and multiply with the frequency distribution given by Eq. (8). The final time domain signal can be obtained by taking the inverse Fourier transform of the RF spectrum under the assumed incident pulse spectrum. An attractive feature of this approach is that after the frequency response is calculated, RF signals for different incident pulses can be obtained easily at this stage without the need to redo the entire simulation.

III. ACCURACY AND EFFICIENCY OF THE FREQUENCY DOMAIN METHOD

To assess the accuracy of the 2D model, we compared computed pulsed waveforms and beam patterns with the same data generated using the FIELD II program. The latter uses the time domain formulation of the Born approximation when modeling the scattered signal waveforms.[13,20] We calculated the pressure field for a 64×64 square array with element dimension of 0.15 mm and center-to-center spacing of 0.2 mm. Furthermore, we assumed a rigid baffle, no apodization, and a speed of sound of 1540 m/s. It was also assumed that each element has a surface velocity that is described by a Gaussian function in time (Fig. 2), with a center frequency of 4 MHz, a 3 dB bandwidth of 2.8 MHz, and unit amplitude. We used a single transmit focus at 30 mm and dynamic receive focus with a F-number set at 2. The pulse-echo field was calculated, and attenuation and dispersion were ignored. The sampling frequency used in FIELD II was 200 MHz to minimize numerical errors due to aliasing of the impulse response.

Figure 3 shows the beam patterns calculated by both the frequency domain model described above and FIELD II. Both are computed for the same transducer geometry, transmit focal distance, and pulsing conditions. Results are presented in the x-z plane for steering angles of 0° and 10°. The results obtained with the two methods match very well.

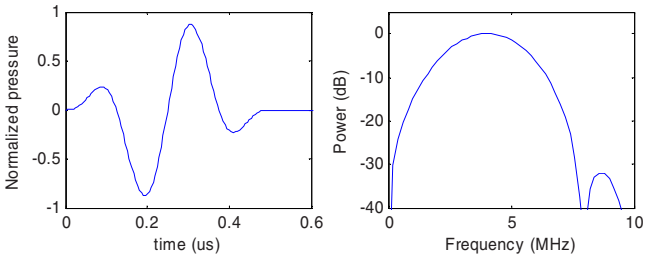

FIG. 2. Assumed velocity waveform and its spectrum from the transducer element surface, used for comparing performance of the frequency domain model with time domain model. The center frequency is 4 MHz and the 3 dB bandwidth is 2.8 MHz.

Figure 4 plots examples of the RF waveforms calculated using the frequency domain method and FIELD II at different depths for a steering angle of 0°. Observe that the results obtained using the two methods are very similar.

To quantitatively evaluate the accuracy of the frequency domain method, we compared the RF waveforms generated by the model with those produced by FIELD II. Thus, for different steering angles and depths, RF waveforms were calculated using both methods. Computations were done at 25 field points within a 5×5 mm^2 region centered at specific locations. At each location, a normal "relative error" was calculated using

$$\text{Error } \% = 100 \times \sqrt{\frac{\sum_{i,j}[V_i(t_j) - V_i^F(t_j)]^2}{\sum_{i,j}[V_i^F(t_j)]^2}}, \tag{10}$$

where $V_i(t_j)$ is the value of the ith waveform sampled at time t_j, and $V_i^F(t_j)$ is the waveform value computed using FIELD II.

Figure 5 plots the relative error between the frequency domain method and FIELD II. Results are shown for four steering angles and 12 distances. Note that the relative error is nearly independent of the steering angle and decreases with distance. For the condition simulated, when the distance is greater than 2 cm, the relative error is smaller than 4% for all steering angles.

The relative efficiency of the two methods was evaluated by comparing the computation time for calculating B-mode images of a simulated phantom using 2D arrays with 16×16, 32×32, and 64×64 active elements. The center frequency applied was 4 MHz and the 3 dB bandwidth was 2 MHz. The phantom simulated has a dimension of $4\times1\times6$ cm^3 and contains 240 000 scatterers. For the frequency domain method, we chose to use 4096 sampling points for each RF A-line, where the sampling rate is taken as 40 MHz. This provides a waveform representing signals over a 7.88 cm depth range. This extends beyond the physical dimensions of the simulated phantom (6 cm height). Thus, we assume the scatterers in the phantom are placed at a depth range of 1 to 7 cm in the simulated phantom. The maximum frequency calculated is 16 MHz, which implies that the cal-

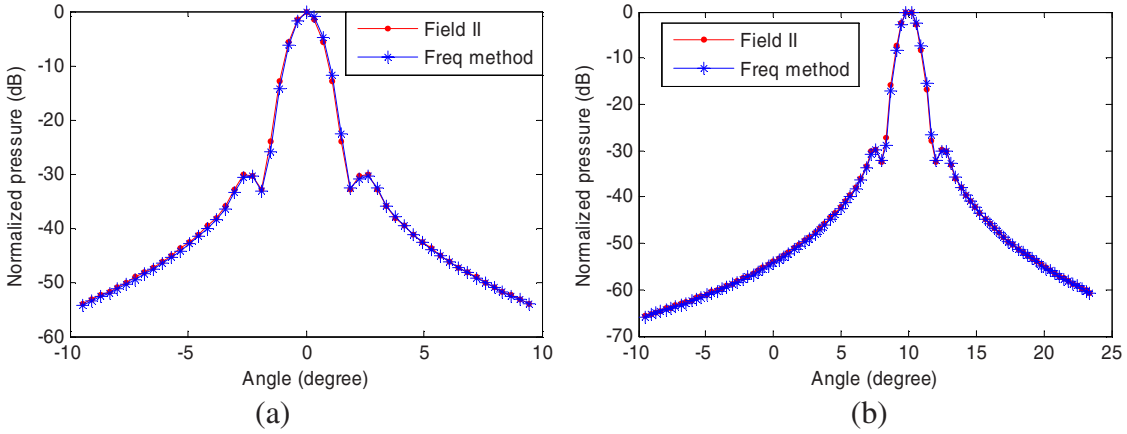

FIG. 3. Beam profiles of the 2D array calculated using the frequency domain method and FIELD II with steering angles of (a) 0° and (b) 10°.

culation has to be done in the frequency domain in 1/256 MHz (16 MHz/4096) increments from 0 to 16 MHz.

Computation times were normalized to the time required for simulating an image with a 2D array having 64×64 active elements calculated by FIELD II. In each case, a single 2D B-mode image containing 400 acoustic scan lines was generated.

Results of this comparison are presented in Fig. 6. Observe that the computation time for FIELD II increases dramatically with an increase in the element number. In contrast, the frequency-domain method indicates a slow increase in the computation time, which is not scaled to the element number. This is because in our simulation, frequency components for forming the echo signals for different beam lines

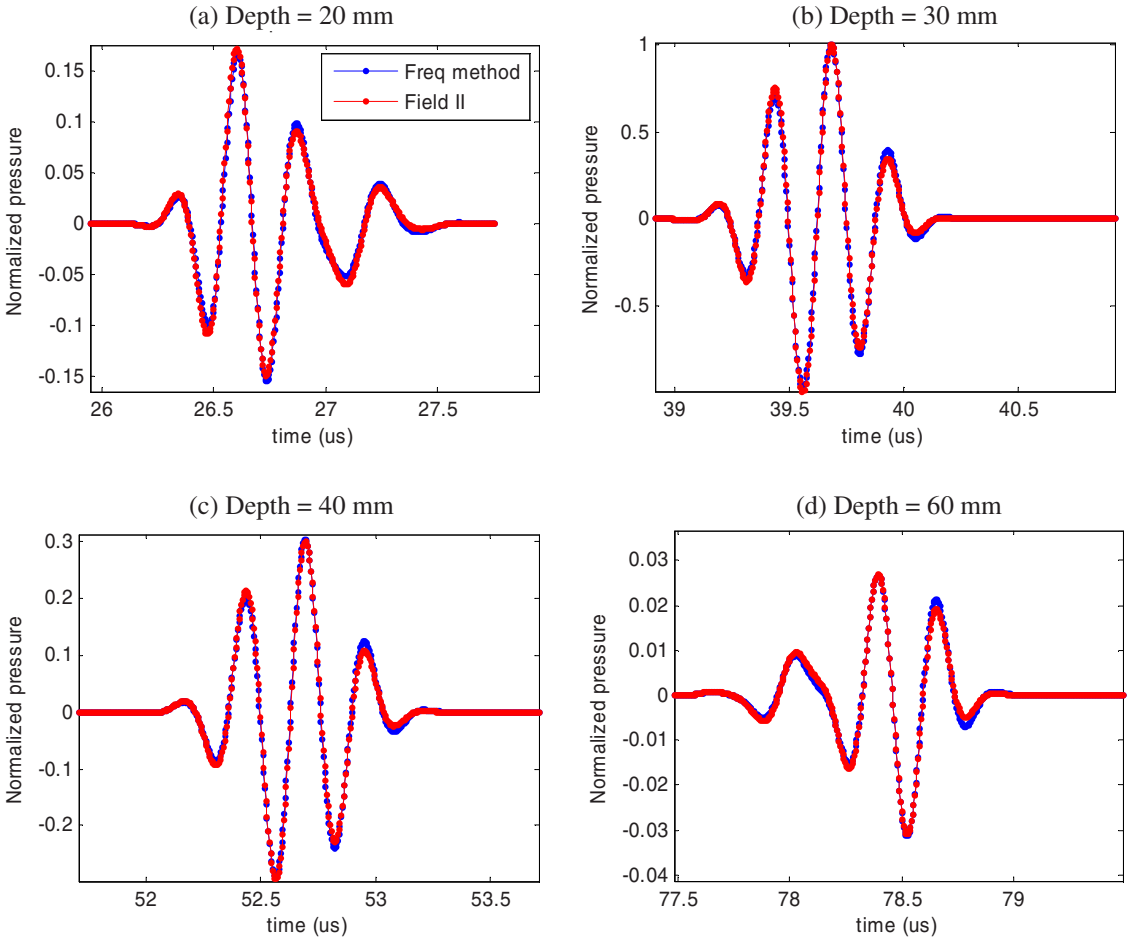

FIG. 4. Pressure waveforms calculated using the frequency domain method and FIELD II at different depths with a steering angle of 0°.

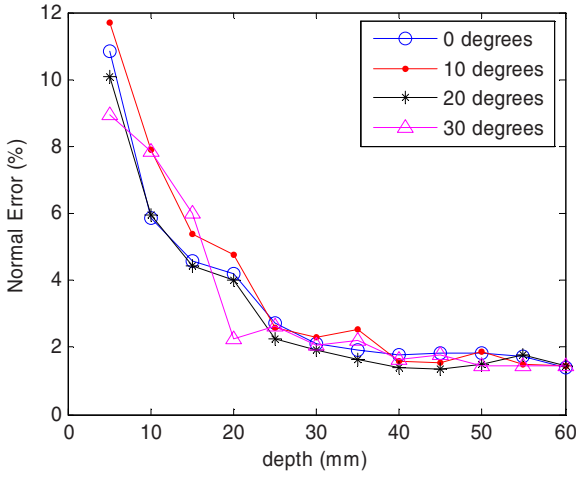

FIG. 5. Comparisons of the relative errors between the frequency domain method and FIELD II at different steering angles and distances computed by Eq. (10).

are calculated by linearly shifting the ultrasound field across the computational phantom. Thus, there is no need to redo the field calculation for each beam line. For the case of the 64×64 array, the frequency-domain method described in this paper is about 35 times faster than FIELD II for producing a B-mode image of the above phantom. The machine used for this test contains a 2.8 GHz CPU and 512 MB of RAM memory. The computation time of the frequency-domain method was about 2 h for a 64×64 array, while FIELD II required 3 days for the same simulation.

IV. EXAMPLE OF USE

The ultrasound simulation model is implemented in C/C++ on a Windows XP platform using the Microsoft Visual C++ compiler. The program makes use of standard library functions only; therefore, it can be ported to any other platform that supports C/C++. We will present images of simulated beam patterns, point spread functions, and B-mode images of lesion phantoms. For all results presented in this paper, the square element utilized for the 2D array elements were modeled with dimensions of 0.15 mm with 0.2 mm spacing between the centers of adjacent elements. The proposed method can also be utilized to simulate high frequency 2D array transducers. The approximations that allow the simplification of the 2D Rayleigh integral hold as long as the dimensions of the element are small enough to satisfy the $a\approx\lambda/2$ requirement. In addition, for the manufacture of higher frequency 2D arrays, newer fabrication technologies can be applied to make very small elements in order to avoid grating lobes.[21–23]

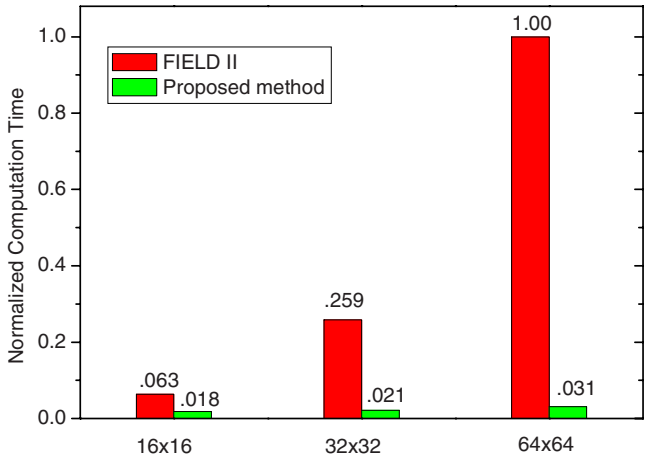

FIG. 6. Comparison of the computation time for the frequency domain method and FIELD II; the time is normalized by the time for 2D arrays with 64×64 active elements calculated by FIELD II.

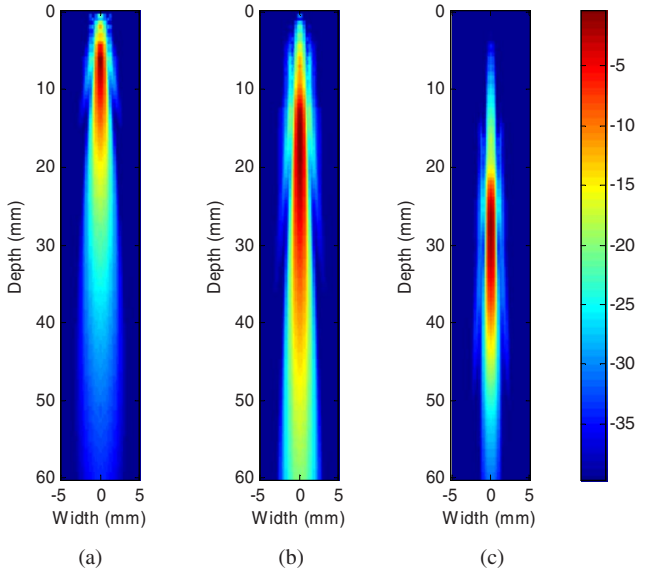

FIG. 7. Pulse-echo beam patterns for a 4 MHz center frequency pulse, generated by the frequency domain model for 2D arrays with (a) 16×16, (b) 32×32, and (c) 64×64 active elements.

IV.A. Beam patterns

Pulse-echo beam profiles may be computed by positioning a single, pointlike scatterer in the field, computing the echo signal for that single scatterer and determining the magnitude of the signal. Figure 7 shows pulse-echo beam patterns obtained by doing this calculation throughout the field using the frequency domain method. Results are shown for 2D arrays having 16×16, 32×32, and 64×64 active elements. A Gaussian-shaped input pulse with a center frequency of 4 MHz was used, and the 6 dB bandwidth was assumed to be 50%. The transmit focus was assumed to be 3 cm and a dynamic receive focus with a constant $F/2$ was used until reaching the limit due to aperture size. The color-scale represents the log-compressed amplitude of the pulse response. Each image is normalized to its own maximum amplitude and the display dynamic range is 40 dB.

IV.B. Point spread functions

Point spread functions for different aperture sizes were generated by simulating images of isolated point targets located at fixed distances along the transmitted beam axis of

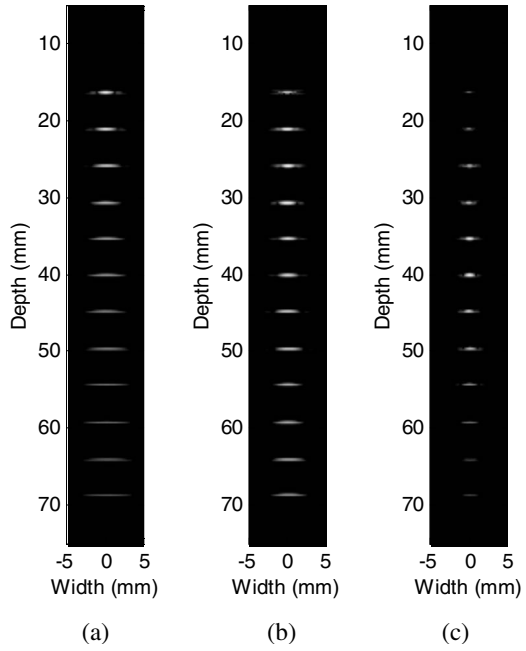

FIG. 8. Images of point spread functions at various depths for a 4 MHz center frequency pulse, generated by the frequency domain model for 2D arrays with (a) 16×16, (b) 32×32, and (c) 64×64 active elements.

the array, then plotting the amplitude vs. lateral distance from the beam axis. We performed these simulations for 2D arrays with 16×16, 32×32, and 64×64 square elements. The pulse implemented is a 4 MHz Gaussian modulated sine wave with a 6 dB bandwidth of 50%. In this example, the transmit focus was assumed to be 4 cm and a dynamic receive focus with a constant $F/2$ was used until reaching the limit due to aperture size. The images in Fig. 8 illustrate the effect of the aperture size on the width of the pulse-echo response. The point spread functions are displayed over a 40 dB dynamic range.

IV.C. B-mode images of lesion phantoms

We also simulated B-mode images from a solid tissue-mimicking phantom containing 23 small spherical "lesions." The phantom material is assumed to have a speed of sound of 1540 m/s and attenuation was assumed to be negligible. Three millimeter diameter spherical, low scatter objects are assumed to be positioned at regular lattice points throughout the scan plane. These were represented by assigning the backscatter levels to 0 within the sphere. The lesion phantom is constructed with scatterers modeled using 40 μm radius polystyrene beads, which are randomly distributed in the phantom at a number density of 10 scatterers per cubic millimeter to ensure Rayleigh statistics.[19] The phantom simulated has dimensions of $4\times2\times6$ cm^3. The lateral and elevational transmit focus was assumed to be 4 cm, and a dynamic receive focus with a constant $F/2$ was used in both the lateral and elevational directions until reaching a limit due to aperture size.

Results obtained using this simulation are presented in Figs. 9(a)–9(c) for aperture sizes of 16×16, 32×32, and 64×64 elements whose dimensions were each 0.15 mm on a side. Figure 9(d)) presents a simulated image for the same 4 MHz pulsing conditions, but generated assuming use of a linear array transducer having a fixed focal length lens in the elevational direction, focused at a depth of 4 cm. The 1D array consists of 64 elements of size 150 μm$\times$12 mm, with a center-to-center distance of 0.2 mm. Note that for 1D transducer arrays, Eq. (5) should not be used to calculate the 2D Rayleigh integral, and the y' integration must be done numerically as described by Li and Zagzebski in Ref. 17. Observe that for 1D arrays the 3 mm objects are visualized at the elevational focus (4 cm), but not detected in the near field or in the far field due to slice thickness effects. The 2D arrays, on the other hand, provide significantly improved resolution at shallower depths when compared to 1D array. The resolution at deeper depths for the 2D arrays is limited by the aperture sizes that were applied in this simulation.

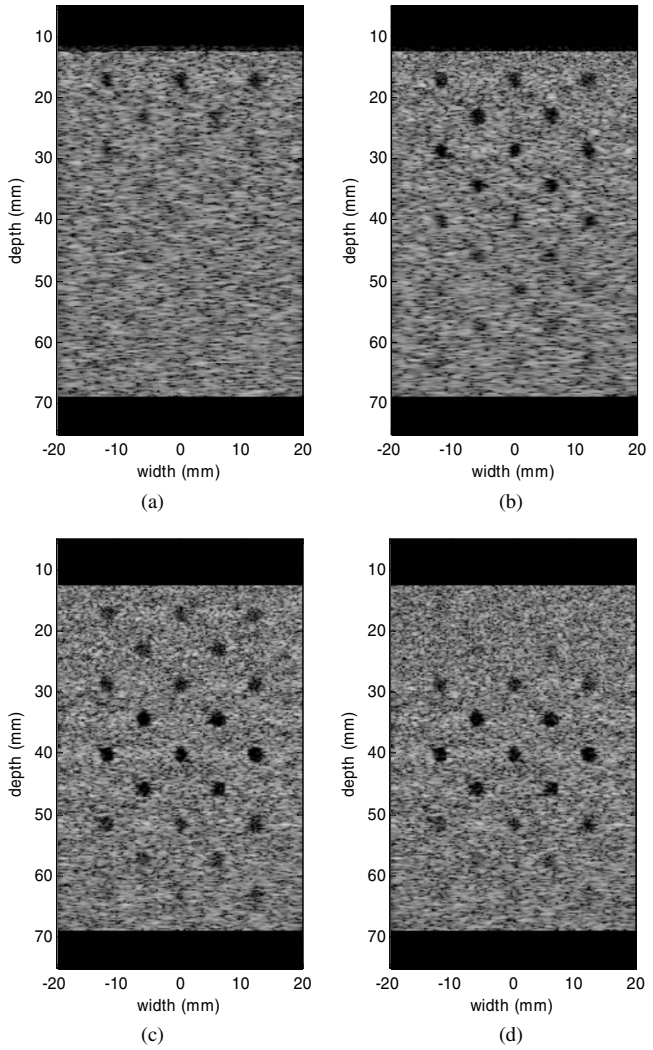

FIG. 9. Simulated B-mode images of a "3 mm spherical lesion" phantom for a 5 MHz center frequency pulse, shown for 2D arrays with (a) 16×16, (b) 32×32, and (c) 64×64 active elements and (d) a 1D array with 64 rectangular elements.

V. DISCUSSION

The 2D arrays provide the capability for electronic steering of ultrasound beams throughout a 3D volume. Thus, they represent a promising solution for implementing real time 3D ultrasound imaging. Because of the complexity of implementing 2D array systems, it is particularly important to develop accurate and efficient image simulation models to investigate how image quality varies with array design and implementation. The plots of beam patterns and point spread function images, such as those shown in Figs. 7 and 8, allow evaluation of beam properties for specific transducer parameters. Simulations of B-mode images also can provide vivid demonstrations of the abilities of 2D arrays and imaging parameters for detecting lesions of a given backscatter contrast and size.

A variety of models for computing beam patterns and generating simulated images from array transducers have been described in the literature. In this paper, we extend the frequency domain model developed by Li and Zagzebski[17] to incorporate 2D arrays. This model is based on a less restrictive near field approximation than the frequently applied Fresnel approximation,[15] and thus maintains excellent accuracy throughout the imaged field. For 2D arrays, since both sides of the array element are small, the method can be further simplified, and the 2D integration generally used in the frequency domain method can be computed using two sinc functions as shown in Eq. (5). Compared with results obtained using the widely used field simulator FIELD II, the frequency domain simulation model using the field approximation shown in Eq. (4) performs very well in terms of accuracy and computational efficiency.

Many ultrasonic properties that must be included in ultrasound field models are frequency dependent, including attenuation, dispersion, and backscatter. These properties appear in the frequency domain formulation simply as multiplicative factors, making it convenient to use a frequency domain model so that these properties can be easily incorporated and their influence on imaging properties studied. For example, attenuation is taken into account by replacing k in Eq. (5) by a complex wave number $K=(\omega/c)+i\alpha(\omega)$, where $\alpha(\omega)$ is the frequency-dependent attenuation coefficient. Typically $\alpha(\omega)$ is a linear or higher order function of the frequency. It has been found that there is almost no change in the computation time when the attenuation effect is included in our model. Previous publications by our group[24–26] have investigated these frequency-dependent features in more detail and demonstrated that they can be handled efficiently using the frequency domain mode. In the time domain, various layers of convolution have to be added to model these frequency-dependent features. Another advantage of the method is that after the field [Eq. (6)] and/or the pulse-echo response [Eq. (8)] are computed over a range of frequencies, RF signals for different incident pulses can be obtained rapidly without the need to redo the simulation.

VI. CONCLUSION

A frequency domain simulation model described previously[17] has been extended to incorporate 2D arrays. Compared with the widely used ultrasound field simulator FIELD II, the model described in this paper is computationally efficient and demonstrates good accuracy for all steering angles. Realistic B-mode images generated using a 2D array transducer can be obtained using this model. Many frequency-dependent imaging parameters and properties are more easily modeled in the frequency domain than in the time domain, so the frequency domain approach provides an effective tool to model transmitted and pulse-echo fields as well as B-mode images for 2D array transducers.

ACKNOWLEDGMENTS

This work is supported by Komen Foundation Grant No. BCTR0601153.

[a]Telephone: (608) 262-8849; Fax: (608) 262-2413; Electronic mail: minrao@wisc.edu

[1]S. W. Smith, H. G. Pavy, and O. T. VonRamm, "High-speed ultrasound volumetric imaging-system.1. Transducer design and beam steering," IEEE Trans. Ultrason. Ferroelectr. Freq. Control **38**, 100–108 (1991).
[2]M. Greenstein, P. Lum, H. Yoshida, and M. S. Seyed-Bolorforosh, "A 2.5 MHz 2D array with Z-axis electrically conductive backing," IEEE Trans. Ultrason. Ferroelectr. Freq. Control **44**, 970–977 (1997).
[3]M. Eames, S. Zhou, and J. Hossack, "High element count (3600) fully sampled, two dimensional transducer array," in Proceedings of IEEE Ultrason. Symposium, Vol. 11, pp. 2243–2246, 2005.
[4]B. Savord and R. Solomon, "Fully sampled matrix transducer for real time 3D ultrasonic imaging," in Proceedings of IEEE Ultrason. Symposium, Vol. 9, pp. 945–953, 2003.
[5]A. Austeng and S. Holm, "Sparse 2-D arrays for 3-D phased array imaging—Design methods," IEEE Trans. Ultrason. Ferroelectr. Freq. Control **49**, 1087–1093 (2002).
[6]G. Cardone, G. Cincotti, and M. Pappalardo, "Design of wide-band arrays for low side-lobe level beam patterns by simulated annealing," IEEE Trans. Ultrason. Ferroelectr. Freq. Control **49**, 1050–1059 (2002).
[7]R. E. Davidsen, J. A. Jensen, and S. W. Smith, "Two-dimensional random arrays for real time volumetric imaging," Ultrason. Imaging **16**, 143–163 (1994).
[8]S. Tezuka, S. Hashimoto, T. Togasaki, Y. Miyajima, and Y. Seo, "A two-dimensional array probe that has a huge number of active channels," in Proceedings of IEEE Ultrason. Symposium, Vol. 1, pp. 960–963, 2003.
[9]G. Thupholme, "Generation of acoustic pulse by baffled plane pistons," Mathematika **16**, 209–224 (1969).
[10]P. Stepanishen, "Transient radiation from pistons in an infinite planar baffle," J. Acoust. Soc. Am. **49**, 1629–1638 (1971).
[11]J. L. San Emeterio and L. G. Ullate, "Diffraction impulse response of rectangular transducers," J. Acoust. Soc. Am. **92**, 651–662 (1992).
[12]J. A. Jensen, "Ultrasound field from triangular apertures," J. Acoust. Soc. Am. **100**, 2049–2056 (1996).
[13]J. A. Jensen and N. B. Svendsen, "Calculation of pressure fields from arbitrarily shaped, apodized and excited ultrasound transducers," IEEE Trans. Ultrason. Ferroelectr. Freq. Control **39**, 262–267 (1992).
[14]D. H. Turnbull and F. Foster, "Beam steering with pulsed two-dimensional transducer arrays," IEEE Trans. Ultrason. Ferroelectr. Freq. Control **38**, 320–333 (1991).
[15]J. W. Goodman, *Introduction to Fourier Optics* (McGraw-Hill, San Francisco, 1968).
[16]P. Crombie, A. Bascom, and S. Cobbold, "Calculating the pulsed response of linear arrays: Accuracy vs. computational efficiency," IEEE Trans. Ultrason. Ferroelectr. Freq. Control **44**, 997–1009 (1997).
[17]Y. Li and J. A. Zagzebski, "A frequency domain model for generating B-mode images with array transducers," IEEE Trans. Ultrason. Ferroelectr. Freq. Control **46**, 690–699 (1999).
[18]P. Morse and K. Ingard, *Theoretical Acoustics* (Princeton University Press, Princeton, NJ, 1986).
[19]R. F. Wagner, S. W. Smith, J. M. Sandrik, and H. Lopez, "Statistics of speckle in ultrasound *B* -scans," IEEE Trans. Sonics Ultrason. **30**, 156–163 (1983).

[20]T. L. Szabo, B. U. Karbeyaz, R. O. Cleveland, and E. L. Miller, "Determining the pulse-echo electromechanical characteristic of a transducer using flat plates and point targets," J. Acoust. Soc. Am. **116**, 90–96 (2004).
[21]A. Caronti, G. Caliano, R. Carotenuto, A. Savoia, M. Pappalardo, E. Cianci, and V. Foglietti, "Capacitive micromachined ultrasonic transducer (CMUT) arrays for medical imaging," Microelectron. J. **37**, 770–777 (2006).
[22]I. G. Mina, H. Kim, I. Kim, S. Kyu, K. Choi, T. N. Jackson, R. L. Tutwiler, and S. Trolier-McKinstry, "Frequency piezoelectric MEMS ultrasound transducers," IEEE Trans. Ultrason. Ferroelectr. Freq. Control **54**, 2422–2430 (2007).
[23]M. Lukacs, J. H. Yin, G. F. Pang, R. C. Garcia, E. Cherin, R. Williams, J. Mehi, and F. S. Foster, "Performance and characterization of new micromachined high-frequency linear arrays," IEEE Trans. Ultrason. Ferroelectr. Freq. Control **53**, 1719–1729 (2006).
[24]Q. Chen and J. A. Zagzebski, "Simulation study of effects of speed of sound and attenuation on ultrasound lateral resolution," Ultrasound Med. Biol. **30**, 1297–1306 (2004).
[25]H. Tu, J. Zagzebski, and Q. Chen, "Attenuation estimations using envelope echo data: Analysis and simulations," Ultrasound Med. Biol. **32**, 377–386 (2006).
[26]W. Liu, J. A. Zagzebski, T. Varghese, A. L. Gerig, and T. J. Hall, "Spectral and scatterer-size correlation during angular compounding: Simulations and experimental studies," Ultrason. Imaging **28**, 230–244 (2006).